Full-field birefringence imaging by thermal-light polarization-sensitive optical coherence tomography. I. Theory — **Source link** ↗

Julien Moreau, V. Loriette, Albert-Claude Boccara

Institutions: Centre national de la recherche scientifique

Related papers:

- Full-field birefringence imaging by thermal-light polarization-sensitive optical coherence tomography. II. Instrument and results

- Determination of birefringence and absolute optic axis orientation using polarization-sensitive optical coherence tomography with PM fibers

- Two-dimensional depth-resolved Mueller matrix characterization of biological tissue by optical coherence tomography.

- Depth-resolved birefringence and differential optical axis orientation measurements with fiber-based polarization-sensitive optical coherence tomography.

- Helical computed tomography with feedback scan control

Full-Field Birefringence Imaging by Thermal-Light Polarization-Sensitive Optical Coherence Tomography. I. Theory

Julien Moreau, V. Loriette, A.C. Boccara

Full-field birefringence imaging by thermal-light polarization-sensitive optical coherence tomography. I. Theory

Julien Moreau, Vincent Loriette, and Albert-Claude Boccara

A method for measuring birefringence by use of thermal-light polarization-sensitive optical coherence tomography is presented. The use of thermal light brings to polarization-sensitive optical coherence tomography a resolution in the micrometer range in three dimensions. The instrument is based on a Linnik interference microscope and makes use of achromatic quarter-wave plates. A mathematical representation of the instrument is presented here, and the detection scheme is described, together with a discussion of the validity domain of the equations used to evaluate the birefringence in the presence of white-light illumination. © 2003 Optical Society of America

OCIS codes: 110.4500, 120.5060, 260.1440.

1. Introduction

The presence of point defects inside multilayer optical coatings is a major source of losses in optical systems that require low levels of scattering. The performance of laser gyros and interferometric detectors of gravitational waves is directly affected by the amount of scattered light that is present; usually scattering levels larger than a few parts in 10^6 are not tolerated.[1,2] Lowering the number of scattering defects inside optical coatings is a technical challenge that requires the development of diagnostic tools in parallel with optimization of the manufacturing processes. The exact localization of point defects inside a multilayer structure, on the substrate–coating interface, at the interface between layers, or inside layers could produce useful information on the source of contamination. However, a single point defect may scatter only a few parts in 10^6 of the flux incident upon the optical component, so a simple tomographic image of the component's reflectance would not permit the detection of such a small signal, which would

be completely masked by the specular reflectances of the various interfaces of the coating. Recently it was proposed to get rid of the specular reflectance signals by performing optical coherence tomography (OCT) measurements on tilted optical components.[3] Another solution could be to detect the change of polarization of the incident light caused by the presence of nonspherical scattering defects. Birefringence imaging has already proved to be a highly efficient way of revealing structures inside various media such as biological and geological specimens. Birefringence signals may be affected by chemical, mechanical, or structural causes, which are usually barely detectable with polarization-insensitive instruments if the causes do not modify the reflectance of the structure. A combination of polarization measurement and OCT has been successfully used to image birefringent structures in biological tissues.[4–12] In these experiments the axial resolution is determined by the coherence length of the source. Usually superluminescent diodes are used, with a coherence length in the 10–20-μm range. The search for micrometer-scale resolution in classic (non-polarization-sensitive) OCT has been achieved either with femtosecond lasers[13] or with the addition of more original superluminescent light sources with bandwidths ten times larger than those of classic superluminescent diodes.[14] Recently, similar resolution was obtained with thermal light.[15] Thermal light may not be so effective as spatially coherent light sources in producing high-sensitivity systems, but it has the advantages of low cost and ease of

The authors are with the École Supérieure de Physique et Chimie Industrielles de la Ville de Paris, Laboratoire d'Optique Physique, Centre National de la Recherche Scientifique Unité Propre de Recherche 5, 10 rue Vauquelin, 75005 Paris, France. V. Loriette's e-mail address is loriette@optique.espci.fr.

implementation on a standard microscope, and, above all, permits the use of detector arrays to perform full-field microscopy.[16-18] To achieve a phase-sensitive (PS) OCT instrument with micrometer resolution in three dimensions we chose to use a thermal light source in a polarization-sensitive Linnik microscope. The detector is a CCD array, and the detection is based on sine phase-modulation interferometry.[19,20] In this paper we present a mathematical description of our instrument. We show that, by making two measurements with different orientations of the polarizing elements, one can characterize the magnitude and direction of birefringence or of dichroism and simultaneously obtain phase OCT images, with limited crossover among the various parameters. Crossover is induced by the use of a polychromatic light source. We show how the spectrum's shape affects the measurements of topography and birefringence and under what hypotheses the equations that are valid for monochromatic illumination can be corrected to be used with polychromatic illumination.

2. Setup

The Linnik microscope (a Michelson interferometer with microscope objectives in both arms) is the instrument of choice to fulfill the requirements of three-dimensional imaging capabilities, lateral and axial resolution in the micrometer range, sensitivity to polarization,[21] and full-field imaging capabilities. The hardest requirement to fulfill is to achieve axial resolution, because it requires working either with high-numerical-aperture objectives[22] or with a broadband source. The second solution is preferred because only standard sets of microscope objectives with relatively low numerical apertures and classic illumination sources can be used. However, in using a broadband source one has to overcome two difficulties: First, perfectly symmetrical arms are necessary to ensure that the resolution is not spoiled by dispersion mismatch. Then, as is the case in most polarization-sensitive interferometers, quarter-wave plates are present inside the arms. The best achromatic quarter-wave plates are Fresnel rhombs, but their use is difficult in this setup because they shift the beams laterally. The only other solution is to use thin achromatic quarter-wave plates, but those plates are achromatic only over a few hundred nanometers. Thermal light sources, such as xenon lamps, have spectral widths larger than 800 nm, whereas typical thin achromatic quarter-wave plates working in the visible spectrum have a spectral width of 300 nm, which limits the width of the usable light spectrum and thus reduces the achievable resolution. Our system is shown schematically in Fig. 1.

3. Measurement Method

In this section we show how we calculate the intensity of the field on the detector and extract information from the sample. We start by recalling a few basic mathematical tools that we shall use throughout our calculations. We perform the calculations
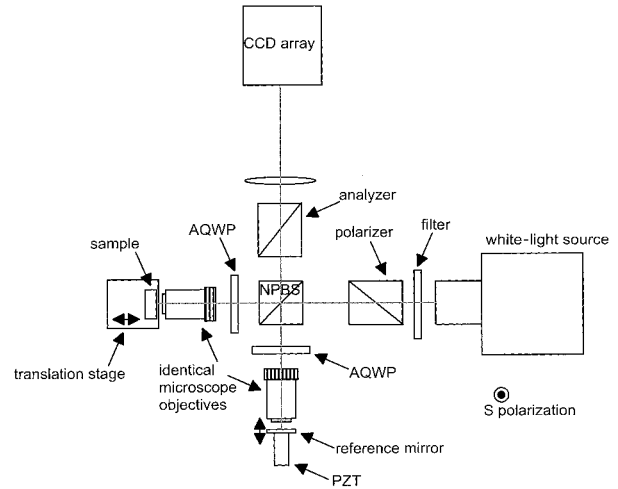

Fig. 1. Schematic of the instrument: NPBS, nonpolarizing beam-splitter cube; AQWPs, achromatic quarter-wave plates; PZT, piezoactuated translation stage.

first for monochromatic and then for broadband illumination. In each case the calculation is divided into two steps: First we calculate a Jones matrix that represents the whole interferometer and show that by making two measurements we can obtain the necessary information with which to evaluate both topographic and birefringence signals. Then we present a measurement method, based on a phase-modulation technique, that permits the topographic and birefringence signals to be recovered from a combination of intensity measurements. We always calculate the field intensity on a pixel that images a finite transverse section of the sample. As the measurement is local (i.e., pixels are independent), we do not explicitly write the dependence on transverse coordinates in the equations. In the following calculations all phase variables are denoted by the Greek letters φ for the phase terms induced by the sample and ϕ for propagation phase terms; all length variables are denoted by either δ for lengths that characterize the sample or Δ for lengths of the arms.

A. Basic Mathematical Tools

The basic tools that we use to calculate the state of polarization of the electromagnetic field in an interferometer are Jones matrices. We do not present the theory behind Jones matrix calculus or calculations of elementary Jones matrices, as they can be found in many textbooks.[23] Jones matrices allow the amplitude of the transverse optical field emerging from a polarizing component to be calculated if the amplitude of the incident transverse field is known. The fields are represented as vectors on an orthonormal basis $(\mathbf{e}_S, \mathbf{e}_P)$. The directions of the transverse vectors are chosen depending on the setup geometry. In the following calculations we refer to S and P linear polarization states. In the instrument those directions are fixed by the orientation of a beam splitter cube. If the beam splitter were a perfectly non-

polarizing component, any other directions could be used; but in practice a so-called nonpolarizing beam splitter always exhibits some polarization properties, and those imperfections can be used to align any other optical axis in the instrument. For example, if a linearly polarized field is incident upon the beam splitter, the reflected and transmitted fields will be slightly elliptically polarized unless the incident field is perfectly parallel or perfectly perpendicular to the plane of incidence on the beam splitter's interface. It is thus natural to define the S polarization state as an electric field vector perpendicular to the plane of incidence on the beam splitter's interface. The basic Jones matrices that we need are the following. M_S and M_P are the Jones matrices of vertical and horizontal polarizers:

$$M_S = \begin{bmatrix} 1 & 0 \\ 0 & 0 \end{bmatrix}, \tag{1}$$

$$M_P = \begin{bmatrix} 0 & 0 \\ 0 & 1 \end{bmatrix}; \tag{2}$$

We have chosen to use positive values for the components of M_R; this means that the reflected field is described on the same $(\mathbf{e}_S, \mathbf{e}_P)$ basis as the incident field, although the direction of the wave vector is reversed on reflection. This choice has no influence on the results, but it simplifies the calculation because, in this case, the Jones matrix that represents a polarizing element with axes that make an angle θ with the basis vectors retains its form, independently of the direction of the field incident upon it. As the goal of the measurement is the detection of changes in electromagnetic field properties of a completely polarized beam on reflection on or inside a sample, we should treat the most general case of a birefringent, dichroic, and absorptive sample, and this would lead to the use of a general Jones matrix.[24] However, we are interested chiefly in the detection of pure birefringence. We thus simplify our calculations by fully treating only this case. M_B is the Jones matrix of a birefringent sample with reflection factor r on the basis of its proper axes:

$$M_B = r \begin{bmatrix} \exp[-i(\varphi_B/2)] & 0 \\ 0 & \exp[+i(\varphi_B/2)] \end{bmatrix}. \tag{8}$$

$$M_{B\beta} = r \begin{bmatrix} \cos^2 \beta \, \exp[-i(\varphi_B/2)] + \sin^2 \beta \, \exp[+i(\varphi_B/2)] & -i \, \sin 2\beta \, \sin(\varphi_B/2) \\ -i \, \sin 2\beta \, \sin(\varphi_B/2) & \cos^2 \beta \, \exp[+i(\varphi_B/2)] + \sin^2 \beta \, \exp[-i(\varphi_B/2)] \end{bmatrix}. \tag{9}$$

M_Q is the Jones matrix of a quarter-wave plate with its fast axis vertical:

$$M_Q = \exp\left(i \frac{\pi}{4}\right) \begin{bmatrix} 1 & 0 \\ 0 & -i \end{bmatrix}; \tag{3}$$

M_θ is the rotation matrix of angle θ in the $(\mathbf{e}_S, \mathbf{e}_P)$ plane:

$$M_\theta = \begin{bmatrix} \cos \theta & \sin \theta \\ -\sin \theta & \cos \theta \end{bmatrix}; \tag{4}$$

$M_{Q\theta}$ is the Jones matrix of a quarter-wave plate with its fast axis making an angle θ with the vertical axis:

$$M_{Q\theta} = M_{-\theta} M_Q M_\theta$$
$$= \exp\left(i \frac{\pi}{4}\right) \begin{bmatrix} \cos^2 \theta - i \sin^2 \theta & \cos \theta \sin \theta (1 + i) \\ \cos \theta \sin \theta (1 + i) & \sin^2 \theta - i \cos^2 \theta \end{bmatrix}; \tag{5}$$

M_{Q45} is the Jones matrix of a quarter-wave plate with its fast axis at 45° from the vertical axis:

$$M_{Q45} = \frac{\sqrt{2}}{2} \begin{bmatrix} 1 & i \\ i & 1 \end{bmatrix}; \tag{6}$$

M_R is the Jones matrix of a nonbirefringent and nondichroic surface with a reflection factor r:

$$M_R = r \begin{bmatrix} 1 & 0 \\ 0 & 1 \end{bmatrix}. \tag{7}$$

Angle φ_B is the phase shift between two orthogonal states of polarization of a field reflected by a structure inside the sample. Its value depends not only on the phase shift induced by the reflection on the structure but also on the birefringence integrated along the round trip of the beam inside the sample. Thus φ_B can be seen not as a local value of birefringence inside a sample but only as an integrated signal. Of course this remark also holds for dichroism and topography of buried structures. $M_{B\beta}$ is the Jones matrix of a birefringent sample on the (S, P) basis; the proper axes make an angle β with the (S, P) axes:

The Jones matrix of a dichroic sample on the basis of its proper axes is

$$M_D = \begin{bmatrix} r_x & 0 \\ 0 & r_y \end{bmatrix}, \tag{10}$$

and on the (S, P) basis

$$M_{D\beta} = \begin{bmatrix} r_x \cos^2 \beta + r_y \sin^2 \beta & (r_x - r_y)\sin \beta \cos \beta \\ (r_x - r_y)\sin \beta \cos \beta & r_x \sin^2 \beta + r_y \cos^2 \beta \end{bmatrix}. \tag{11}$$

In Eq. (11) the reflection factors may be complex; in this case the sample is also birefringent but the axes of birefringence are the same as the axes of dichroism. We use this matrix to represent our sample and, de-

pending on the relative phase and magnitude of r_x and r_y, we shall present either a dichroic or birefringent sample.

$M_{\mathrm{bs}R}$ and $M_{\mathrm{bs}T}$ are the reflection and transmission matrices, respectively, of a perfect nonpolarizing

$$M_{\mathrm{ech}} = M_{\mathrm{bs}R} M_{Q45} M_{S\beta} M_{Q45} M_{\mathrm{bs}T}, \tag{17}$$

$$M_{\mathrm{sam}} = \frac{1}{2} \begin{bmatrix} (r_x - r_y)\exp(2i\beta) & i(r_x + r_y) \\ i(r_x + r_y) & -(r_x - r_y)\exp(-2i\beta) \end{bmatrix} r_{\mathrm{bs}} t_{\mathrm{bs}} \exp(i\phi_{\mathrm{sam}}). \tag{18}$$

beam splitter cube:

$$M_{\mathrm{bs}R} = r_{\mathrm{bs}} \begin{bmatrix} 1 & 0 \\ 0 & 1 \end{bmatrix}, \tag{12}$$

assumption is justified by the fact that in practice the reference mirror is a superpolished flat with a rms roughness less than 0.1 nm. Therefore ϕ_{ref} depends only on the reference mirror's position, $\phi_{\mathrm{ref}} = 4\pi\nu\Delta_{\mathrm{ref}/c}$. The Jones matrix of the sample arm is

For a birefringent sample $r_x + r_y = 2r\cos(\varphi_B/2)$ and $r_x - r_y = -2ri\sin(\varphi_B/2)$. The Jones matrix for the sample arm of length Δ_{sam} reads as

$$M_{\mathrm{sam}} = i \begin{bmatrix} -\sin(\varphi_B/2)\exp(2i\beta) & \cos(\varphi_B/2) \\ \cos(\varphi_B/2) & \sin(\varphi_B/2)\exp(-2i\beta) \end{bmatrix} r_{\mathrm{bs}} t_{\mathrm{bs}} r \exp(i\phi_{\mathrm{sam}}). \tag{19}$$

$$M_{\mathrm{bs}T} = t_{\mathrm{bs}} \begin{bmatrix} 1 & 0 \\ 0 & 1 \end{bmatrix}. \tag{13}$$

The Jones vector of a P-polarized field of intensity I is

$$E_P = \sqrt{I} \begin{pmatrix} 0 \\ 1 \end{pmatrix}. \tag{14}$$

B. Monochromatic Source

1. *Jones Representation of the Arms*

To calculate the field amplitude on the detector we build a single Jones matrix that represents the whole interferometer, using the elementary Jones matrices presented in Subsection 3.A. This matrix is the sum of two matrices, M_{ref} and M_{sam}, that represent, respectively, the reference arm and the sample arm. Although we use a broadband source to obtain the required resolution, it is useful to start the calculations with a monochromatic source. In this way we can deal with much simpler formulas and get better insight into the problem. The broadband source is treated next.

The Jones matrix of a reference arm of length Δ_{ref} is

$$M_{\mathrm{ref}} = M_{\mathrm{bs}T} M_{Q\theta} M_R M_{Q\theta} M_{\mathrm{bs}R}, \tag{15}$$

$$M_{\mathrm{ref}} = i \begin{bmatrix} \cos 2\theta & \sin 2\theta \\ \sin 2\theta & -\cos 2\theta \end{bmatrix} r_{\mathrm{bs}} t_{\mathrm{bs}} r_{\mathrm{ref}} \exp(i\phi_{\mathrm{ref}}). \tag{16}$$

The global phase term ϕ_{ref} represents the phase shift of the field after a round trip in the reference arm. Although is should be sensitive to the topography of the reference mirror as well as to the modulation of its position, as is explicitly detailed below, the reference mirror is assumed to be perfectly flat. This

The global phase term ϕ_{sam} is the phase shift of the field after a round trip in the sample arm.

2. *Field on the Detector for the Monochromatic Source*

The field incident upon the beam splitter is P polarized. To extract the amplitude of the birefringence (or the dichroism) and the direction of the axes we must make two measurements with two orientations of the analyzer. The first measurement is performed with a P-oriented analyzer. The amplitude of the field on the detector is given by

$$E_{\mathrm{det}}^{(P)} = M_P (M_{\mathrm{ref}} + M_{\mathrm{sam}}) E_P. \tag{20}$$

Using Eqs. (14), (18), and (19) in Eq. (20) and using a perfectly symmetrical beam splitter with $r_{\mathrm{bs}} = t_{\mathrm{bs}} = \sqrt{2}/2$, we obtain

$$E_{\mathrm{det}}^{(P)} = \frac{\sqrt{I}}{2} \left[-r_{\mathrm{ref}} \cos 2\theta \, \exp(i\phi_{\mathrm{ref}}) \right.$$
$$\left. - \frac{r_x - r_y}{2} \exp(-2i\beta)\exp(i\phi_{\mathrm{sam}}) \right]. \tag{21}$$

The intensity is thus

$$I_{\mathrm{det}}^{(P)} = \frac{I}{4} (r_{\mathrm{ref}} \cos 2\theta)^2 + \frac{|r_x - r_y|^2}{4} + r_{\mathrm{ref}} \cos 2\theta [\mathrm{Re}(r_x$$
$$- r_y)\cos(\phi - 2\beta) - \mathrm{Im}(r_x - r_y)\sin(\phi - 2\beta)]. \tag{22}$$

Phase $\phi = \phi_{\mathrm{sam}} - \phi_{\mathrm{ref}}$ is the phase shift between the two beams. It is different for each pixel. We can write it by making the topography appear explicitly as

$$\phi(x, y) = \overline{\phi_{\mathrm{sam}} - \phi_{\mathrm{ref}}} + \varphi_z(x, y). \tag{23}$$

The (x, y) coordinates are lateral coordinates on the sample. $\varphi_z(x, y)$ is the classic topography phase signal, $\varphi_z(x, y) = 4\pi\nu\delta_z(x, y)/c$, where $\delta_z(x, y)$ is the sample topography. $\overline{\phi_{sam} - \phi_{ref}} = 4\pi\nu(\Delta_{sam} - \Delta_{ref})/c$ is the phase shift averaged over the (x, y) image field. It is important to insist on the fact that, if an interference term is generated by birefringence or dichroism, then its phase depends not only on the direction of the principal axis β but also on the sample's topography δ_z. Unless a pure topography map of the sample is available, it is not possible to extract the value of the direction of the birefringence–dichroism axes independently of the value of δ_z with only one measurement.

The second measurement is performed with an S-oriented analyzer. In this case we obtain

$$E_{\det}^{(S)} = \frac{\sqrt{I}}{2}\left[r_{ref} \sin 2\theta \, \exp(i\phi_{ref}) \right.$$
$$\left. + i \, \frac{r_x + r_y}{2} \exp(i\phi_{sam}) \right] \tag{24}$$

and, for the intensity,

$$I_{\det}^{(S)} = \frac{I}{4}\left\{ (r_{ref} \sin 2\theta)^2 + \frac{|r_x + r_y|^2}{4} \right.$$
$$- r_{ref} \sin 2\theta[\mathrm{Re}(r_x + r_y)\sin(\phi) + \mathrm{Im}(r_x$$
$$\left. + r_y)\cos(\phi)] \right\}. \tag{25}$$

For a dichroic sample we write $r_x + r_y = 2r_{sam}$ and $r_x - r_y = \delta r$; Eqs. (22) and (25) can be rewritten as

$$I_{\det}^{(P)} = \frac{I}{4}\left[(r_{ref} \cos 2\theta)^2 + \frac{\delta r^2}{4} + r_{ref}\delta r \cos 2\theta \cos(\phi \right.$$
$$\left. - 2\beta) \right], \tag{26}$$

$$I_{\det}^{(S)} = \frac{I}{4}\left[(r_{ref} \sin 2\theta)^2 + r_{sam}^2 \right.$$
$$\left. - 2r_{ref}r_{sam} \sin 2\theta \, \sin(\phi) \right]. \tag{27}$$

When the sample is birefringent, $r_x + r_y = 2r \cos(\varphi_B/2)$ and $r_x - r_y = -2ri \sin(\varphi_B/2)$, Eqs. (22) and (25) can be rewritten as

$$I_{\det}^{(P)} = \frac{I}{4}\left[(r_{ref} \cos 2\theta)^2 + \left(r_{sam} \sin \frac{\varphi_B}{2} \right)^2 \right.$$
$$\left. + 2r_{ref}r_{sam} \cos 2\theta \sin \frac{\varphi_B}{2} \sin(\phi - 2\beta) \right], \tag{28}$$

$$I_{\det}^{(S)} = \frac{I}{4}\left[(r_{ref} \sin 2\theta)^2 + \left(r_{sam} \cos \frac{\varphi_B}{2} \right)^2 \right.$$
$$\left. - 2r_{ref}r_{sam} \sin 2\theta \cos \frac{\varphi_B}{2} \sin(\phi) \right]. \tag{29}$$

Using Eq. (23), we write the results of the two measurements as

$$I_{\det}^{(P)} = I_0^{(P)} + A^{(P)} \cos(\overline{\phi_{sam} - \phi_{ref}})$$
$$+ B^{(P)} \sin(\overline{\phi_{sam} - \phi_{ref}}), \tag{30}$$

$$I_{\det}^{(S)} = I_0^{(S)} + A^{(S)} \cos(\overline{\phi_{sam} - \phi_{ref}})$$
$$+ B^{(S)} \sin(\overline{\phi_{sam} - \phi_{ref}}), \tag{31}$$

with

$$I_0^{(P)} = \frac{1}{4} I \left[(r_{ref} \cos 2\theta)^2 + \left(r_{sam} \sin \frac{\varphi_B}{2} \right)^2 \right], \tag{32}$$

$$A^{(P)} = +\frac{I}{2} r_{ref}r_{sam} \cos 2\theta \sin \frac{\varphi_B}{2} \sin(\varphi_z - 2\beta), \tag{33}$$

$$B^{(P)} = +\frac{I}{2} r_{ref}r_{sam} \cos 2\theta \sin \frac{\varphi_B}{2} \cos(\varphi_z - 2\beta), \tag{34}$$

$$I_0^{(S)} = \frac{1}{4} I \left[(r_{ref} \sin 2\theta)^2 + \left(r_{sam} \cos \frac{\varphi_B}{2} \right)^2 \right], \tag{35}$$

$$A^{(S)} = -\frac{I}{2} r_{ref}r_{sam} \sin 2\theta \cos \frac{\varphi_B}{2} \sin(\varphi_z), \tag{36}$$

$$B^{(S)} = -\frac{I}{2} r_{ref}r_{sam} \sin 2\theta \cos \frac{\varphi_B}{2} \cos(\varphi_z). \tag{37}$$

To measure the amplitude of the birefringence signal we must first extract the four values $A^{(P)}$, $B^{(P)}$, $A^{(S)}$, and $B^{(S)}$. Then the birefringence amplitude can be calculated from

$$\tan^2\left(\frac{\varphi_B}{2} \right) = \tan^{-2}(2\theta) \frac{A^{(P)2} + B^{(P)2}}{A^{(S)2} + B^{(S)2}}; \tag{38}$$

the topography from

$$\tan(\varphi_z) = \frac{A^{(S)}}{B^{(S)}}; \tag{39}$$

and the birefringence direction from

$$\tan(2\beta) = \frac{A^{(S)}B^{(P)} - A^{(P)}B^{(S)}}{B^{(S)}B^{(P)} + A^{(S)}A^{(P)}}. \tag{40}$$

The value of φ_B is of course independent of θ and, in most papers that treat polarization-sensitive OCT experiments, $\theta = \pi/8$. This configuration is useful if the birefringence amplitude is unknown and can *a priori* take any value. We prefer to leave the value of θ unspecified because in some cases, for example, when one is testing nonbiological samples, the birefringence may be small everywhere. In these cases, choosing a lower value for θ enhances the weight of the $\sin(\varphi_B/2)$ terms and thus the signal-to-noise ratio.

3. Modulation
In this last step of the calculation we describe a practical way to compute the values of $A^{(P)}$, $B^{(P)}$, $A^{(S)}$, and $B^{(S)}$. These values can be obtained from

Eqs. (30) and (31) by use of a different set of values for $\overline{\phi_{\text{sam}} - \phi_{\text{ref}}}$ and by calculation of different linear combinations of those results. Four values are necessary to produce a set of two parameters, $A^{(P)}$ and $B^{(P)}$ or $A^{(S)}$ and $B^{(S)}$. One might think that only two values would be necessary, but, as we make clear below, two extra parameters appear, a phase shift and a modulation depth, that need to be evaluated too. We can change $\overline{\phi_{\text{sam}} - \phi_{\text{ref}}}$, for example, by moving the reference mirror to any of four positions. We chose to modulate the reference arm's length sinusoidally with angular frequency ω. This signal extraction method can be used only if the reference mirror's position span is shorter than the depth of field of the microscope objectives; otherwise different positions of the reference mirror will lead not only to a different state of interference but also to a different contrast of the interference signal. An expression of the FWHM of the contrast function can be found in Ref. 22:

$$\text{FWHM} = \frac{0.6\lambda}{1 - \cos(\arcsin \text{N.A.})}, \qquad (41)$$

where N.A. is the numerical aperture of the objective and λ is the wavelength. In practice the modulation amplitude is always smaller than this length because one great advantage of a broadband source is the possibility of using objectives with a depth of field large compared to the average wavelength, because the axial resolution is limited by the coherence length. By using objectives with numerical apertures smaller than 0.6 we can assume that the contrast does not depend on the position of the reference mirror.

We write $\overline{\phi_{\text{sam}} - \phi_{\text{ref}}}$ as

$$\overline{\phi_{\text{sam}} - \phi_{\text{ref}}} = \phi_0 \sin(\omega t + \psi), \qquad (42)$$

where ϕ_0 is the modulation depth and phase term ψ is the phase shift between the reference mirror's modulated position and the CCD acquisition sequence. These two parameters are in practice tunable by electronic means. The constraint that

$$\phi_0 < 2\pi \qquad (43)$$

ensures that the modulation amplitude is small compared to the depth of field of the objective:

$$\sin(\overline{\phi_{\text{sam}} - \phi_{\text{ref}}}) = 2 \sum_{k=0}^{\infty} J_{2k+1}(\phi_0)\sin[(2k+1)(\omega t + \psi)], \qquad (44)$$

$$\cos(\overline{\phi_{\text{sam}} - \phi_{\text{ref}}}) = J_0(\phi_0) + 2 \sum_{k=1}^{\infty} J_{2k}(\phi_0)\cos[2k(\omega t + \psi)]. \qquad (45)$$

The CCD array used to image the sample integrates the signal, so we cannot directly extract the signal at the modulation frequency. Instead, we use the integration property of the detector to acquire four con-
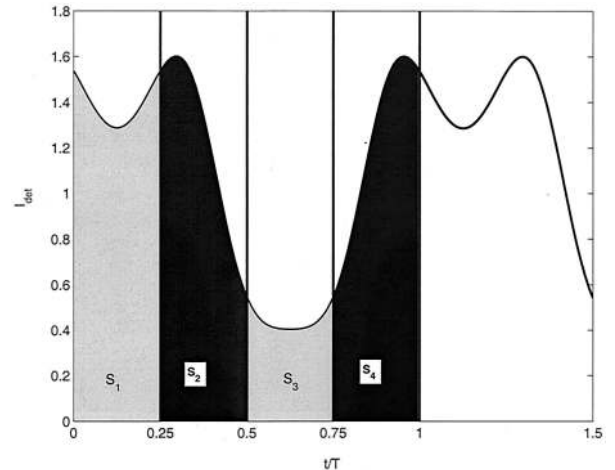

Fig. 2. Typical interferometric signal I_{det} recorded by a CCD pixel as a function of time. This signal is integrated over four consecutive quarters of the modulation period to give four images, S_1–S_4.

secutive images, labeled S_1–S_4, integrated during one quarter of modulation period T. Figure 2 is a simulated signal recorded on one pixel of the CCD array:

$$S_q^{(P)} = \int_{(q-1)T/4}^{qT/4} I_{\text{det}}^{(P)}(t)\mathrm{d}t,$$

$$S_q^{(S)} = \int_{(q-1)T/4}^{qT/4} I_{\text{det}}^{(S)}(t)\mathrm{d}t. \qquad (46)$$

Substituting Eqs. (42), (44), and (30) into Eq. (46), we have

$$\begin{aligned} S_q^{(P)} = {} & \frac{T}{4}\left[I_0^{(P)} + J_0(\phi_0)A^{(P)}\right] \\ & + \frac{TA^{(P)}}{\pi}\sum_{k=1}^{\infty}\frac{J_{2k}(\phi_0)}{2k}\left(\sin\left[2k\left(q\frac{\pi}{2}+\psi\right)\right]\right. \\ & \left. - \sin\left\{2k\left[(q-1)\frac{\pi}{2}+\psi\right]\right\}\right) \\ & - \frac{TB^{(P)}}{\pi}\sum_{k=0}^{\infty}\frac{J_{2k+1}(\phi_0)}{2k+1}\left(\cos\left[(2k+1)\left(q\frac{\pi}{2}\right.\right.\right. \\ & \left.\left.\left. +\psi\right)\right] - \cos\left\{(2k+1)\left[(q-1)\frac{\pi}{2}+\psi\right]\right\}\right), \end{aligned} \qquad (47)$$

and, using Eq. (31), we obtain a similar expression for $S_q^{(S)}$. To extract $A^{(P)}$ and $B^{(P)}$ we use two different linear combinations of the four values of $S_q^{(P)}$:

$$\Sigma_B^{(P)} = -S_1^{(P)} + S_2^{(P)} + S_3^{(P)} - S_4^{(P)}, \qquad (48)$$

$$\Sigma_A^{(P)} = -S_1^{(P)} + S_2^{(P)} - S_3^{(P)} + S_4^{(P)}. \qquad (49)$$

Substituting Eq. (47) into Eqs. (48) and (49) leads to

$$\Sigma_B^{(P)} = \frac{4T}{\pi} B^{(P)} \Gamma_B(\phi_0, \psi), \qquad (50)$$

$$\Sigma_A^{(P)} = \frac{4T}{\pi} A^{(P)} \Gamma_A(\phi_0, \psi), \qquad (51)$$

with

$$\Gamma_B(\phi_0, \psi) = \sum_{k=0}^{\infty} (-1)^k \frac{J_{2k+1}(\phi_0)}{2k+1} \sin[(2k+1)\psi], \quad (52)$$

$$\Gamma_A(\phi_0, \psi) = \sum_{k=1}^{\infty} [1 - (-1)^k] \frac{J_{2k}(\phi_0)}{2k} \sin(2k\psi). \qquad (53)$$

We use the same combinations to extract $A^{(S)}$ and $B^{(S)}$. Equation (38) can thus be rewritten as

$$\tan^2\left(\frac{\varphi_B}{2}\right) = \tan^{-2}(2\theta) \frac{[\Gamma_B(\phi_0, \psi)\Sigma_A^{(P)}]^2 + [\Gamma_A(\phi_0, \psi)\Sigma_B^{(P)}]^2}{[\Gamma_B(\phi_0, \psi)\Sigma_A^{(S)}]^2 + [\Gamma_A(\phi_0, \psi)\Sigma_B^{(S)}]^2}. \qquad (54)$$

4. Evaluation of Modulation Depth ϕ_0 and Modulation Phase ψ

To calculate the value of $\Gamma_A(\phi_0, \psi)$ and $\Gamma_B(\phi_0, \psi)$ we need to measure ϕ_0 and ψ. We could rely on a precise calibration of the reference mirror's displacement system to obtain ϕ_0, but we have no easy way to measure ψ. To overcome this difficulty we need to use other combinations of images to fix those parameters to known values. Once those values are known, we can modify them to optimize the signal-to-noise ratio. As they are independent of the orientation of the analyzer, we can choose to measure them with a P-oriented analyzer. We use the following notation for the image background:

$$S_0^{(P)} = \frac{T}{4} [I_0^{(P)} + J_0(\phi_0)A^{(P)}]. \qquad (55)$$

The four images can be written as

$$S_1^{(P)} = S_0^{(P)} + \frac{T}{\pi} [-A^{(P)}\Gamma_A(\phi_0, \psi) - B^{(P)}f_2(\phi_0, \psi)], \quad (56)$$

$$S_2^{(P)} = S_0^{(P)} + \frac{T}{\pi} [A^{(P)}\Gamma_A(\phi_0, \psi) - B^{(P)}f_3(\phi_0, \psi)], \quad (57)$$

$$S_3^{(P)} = S_0^{(P)} + \frac{T}{\pi} [-A^{(P)}\Gamma_A(\phi_0, \psi) + B^{(P)}f_2(\phi_0, \psi)], \quad (58)$$

$$S_4^{(P)} = S_0^{(P)} + \frac{T}{\pi} [A^{(P)}\Gamma_A(\phi_0, \psi) + B^{(P)}f_3(\phi_0, \psi)], \quad (59)$$

with

$$f_2(\phi_0, \psi) = \sum_{k=0}^{\infty} \frac{J_{2k+1}(\phi_0)}{2k+1} \{\cos[(2k+1)\psi] + (-1)^k \sin[(2k+1)\psi]\}, \qquad (60)$$

$$f_3(\phi_0, \psi) = \sum_{k=0}^{\infty} \frac{J_{2k+1}(\phi_0)}{2k+1} \{\cos[(2k+1)\psi] - (-1)^k \sin[(2k+1)\psi]\}. \qquad (61)$$

It is easy to show that

$$\Gamma_B(\phi_0, \psi) = \frac{1}{2}[f_2(\phi_0, \psi) - f_3(\phi_0, \psi)]. \qquad (62)$$

A practical way to find a specific value of ψ is to tune it until the two images S_2 and S_4 become identical. At this point the value of $f_3(\phi_0, \psi)$ vanishes. If this holds for any value of ϕ_0, which we check by changing the modulation amplitude, then necessarily $\psi = \pi/4$. We can then compute $\Sigma_A^{(P)2} + \Sigma_B^{(P)2}$:

$$\Sigma_A^{(P)2} + \Sigma_B^{(P)2} = \left(\frac{4T}{\pi}\right)^2 \{[A^{(P)}\Gamma_A(\phi_0, \psi)]^2 + [B^{(P)}\Gamma_B(\phi_0, \psi)]^2\}. \qquad (63)$$

Then to fix the value of ϕ_0 we use the fact that, when $\phi_0 = 2.0759$ rad [when $\Gamma_A(\phi_0, \psi) = \Gamma_B(\phi_0, \psi)$], we obtain

$$\Sigma_A^{(P)2} + \Sigma_B^{(P)2}$$
$$= \left[\frac{4T}{\pi} \Gamma_A(\phi_0, \psi) \frac{I}{2} r_{\text{ref}} r_{\text{sam}} \cos 2\theta \sin \frac{\varphi_B}{2}\right]^2, \quad (64)$$

which is obviously independent of the topography signal. In practice one generates a topography signal by tilting the reference mirror such as to get many fringes in the images and then adjusts ϕ_0 to eliminate this topography signal by making the fringes vanish. So, although we do not directly measure ϕ_0 and ψ, we can calculate φ_B by from

$$\tan^2\left(\frac{\varphi_B}{2}\right) = \tan^{-2}(2\theta) \frac{\Sigma_A^{(P)2} + \Sigma_B^{(P)2}}{\Sigma_A^{(S)2} + \Sigma_B^{(S)2}}. \qquad (65)$$

C. Broadband Source

We can now study the case of a broadband source, with an apparent spectrum $f(\nu)$. In what follows, all numerical examples are calculated with a sample spectrum that is flat from 650 to 950 nm. The birefringence amplitude depends on wavelength, and we write $\varphi_B(\nu) = 2\pi\nu\delta_B/c$. The direction of birefringence axes β is a geometrical characteristic of the

sample, which depends mainly on the local orientation of the structures that compose it. We make the hypothesis that within a given structure the directions of the birefringence axes do not change significantly with wavelength. Our goal is to obtain an equation, similar to Eq. (54), that will allow us to evaluate δ_B by using combinations of the eight images. As for the monochromatic source, we first have to find a way to measure the modulation parameters. When the beam splitter, the reference mirror, the quarter-wave plates, and the polarizers are perfectly achromatic, we can write Eqs. (28) and (29) with an explicit dependence on ν as

$$I_{det}^{(P)}(\nu) = \frac{I}{4}\left\{(r_{ref}\cos 2\theta)^2 + \left[r_{sam}\sin\frac{\varphi_B(\nu)}{2}\right]^2\right.$$

$$+ 2r_{ref}r_{sam}\cos 2\theta \sin\frac{\varphi_B(\nu)}{2}\sin[\phi(\nu)]$$

$$\left. - 2\beta\right\}, \qquad (66)$$

$$I_{det}^{(S)}(\nu) = \frac{I}{4}\left\{(r_{ref}\sin 2\theta)^2 + \left[r_{sam}\cos\frac{\varphi_B(\nu)}{2}\right]^2\right.$$

$$\left. - 2r_{ref}r_{sam}\sin 2\theta \cos\frac{\varphi_B(\nu)}{2}\sin[\phi(\nu)]\right\}. \qquad (67)$$

Modulation phase ψ does not depend on wavelength but the modulation depth does, as $\phi_0 = 4\pi\nu\delta_0/c$, where δ_0 is the oscillation amplitude of the reference mirror. The four images are now

$$S_1^{(P)} = S_0^P + \frac{T}{\pi}\left[-\int_0^\infty f(\nu)A^{(P)}(\nu, \delta_B)\Gamma_A(\nu, \delta_0, \psi)d\nu\right.$$

$$\left. - \int_0^\infty f(\nu)B^{(P)}(\nu, \delta_B)f_2(\nu, \delta_0, \psi)d\nu\right], \qquad (68)$$

$$S_2^{(P)} = S_0^P + \frac{T}{\pi}\left[\int_0^\infty f(\nu)A^{(P)}(\nu, \delta_B)\Gamma_A(\nu, \delta_0, \psi)d\nu\right.$$

$$\left. - \int_0^\infty f(\nu)B^{(P)}(\nu, \delta_B)f_3(\nu, \delta_0, \psi)d\nu\right], \qquad (69)$$

$$S_3^{(P)} = S_0^P + \frac{T}{\pi}\left[-\int_0^\infty f(\nu)A^{(P)}(\nu, \delta_B)\Gamma_A(\nu, \delta_0, \psi)d\nu\right.$$

$$\left. + \int_0^\infty f(\nu)B^{(P)}(\nu, \delta_B)f_2(\nu, \delta_0, \psi)d\nu\right], \qquad (70)$$

$$S_4^{(P)} = S_0^P + \frac{T}{\pi}\left[\int_0^\infty f(\nu)A^{(P)}(\nu, \delta_B)\Gamma_A(\nu, \delta_0, \psi)d\nu\right.$$

$$\left. + \int_0^\infty f(\nu)B^{(P)}(\nu, \delta_B)f_3(\nu, \delta_0, \psi)d\nu\right]. \qquad (71)$$
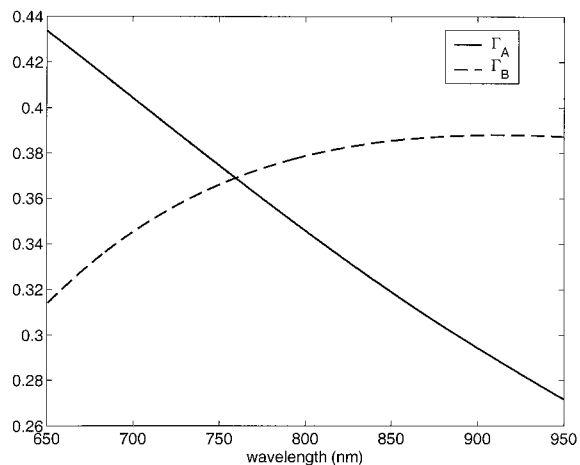
Fig. 3. Values of Γ_A and Γ_B as a function of wavelength for $\delta_0 = \delta_{0opt}$.

We cannot at this point use the equations that are valid for the monochromatic source. The result would not be a measurement of the birefringence weighted by the source spectrum, even if there were no topography signal ($\delta_z = 0$), because the functions Γ_A and Γ_B vary significantly with wavelength, as can be seen from Fig. 3, and thus cannot be extracted from the integrals of Eqs. (68)–(71).

D. Evaluation of Oscillation Amplitude δ_0 and Modulation Phase ψ for the Broadband Source

To fix the values of δ_0 and ψ we perform the same operations as for the monochromatic source. For ψ the problem is simply solved because $f_3(\nu, \delta_0, \pi/4) = 0 \forall \nu, \delta_0$. So, by making $S_2^{(P)} = S_4^{(P)}$, we obtain $\psi = \pi/4$. It is more difficult to handle δ_0, and in fact there is no way to cancel $S_2^{(P)} - S_1^{(P)}$ for any wavelength or for $\Sigma_A^{(S)2} + \Sigma_B^{(S)2}$ to be independent of the topography for any wavelength. We establish the setting by using a nonbirefringent sample and working with an S-oriented analyzer:

$$\Sigma_A^{(S)2} + \Sigma_B^{(S)2} = \left(\frac{4T}{\pi}\right)^2\left(\left\{\int_0^\infty f(\nu)A^{(S)}\right.\right.$$

$$\times (\nu, \delta_B)\Gamma_A[(\nu, \delta_0, \psi)]d\nu\right\}^2$$

$$+ \left\{\int_0^\infty f(\nu)B^{(S)}\right.$$

$$\left.\left. \times (\nu, \delta_B)\Gamma_B[(\nu, \delta_0, \psi)]d\nu\right\}^2\right), \qquad (72)$$

with

$$A^{(S)}(\nu, \delta_B) = -\frac{I}{2}r_{ref}r_{sam}\sin 2\theta \sin(4\pi\nu\delta_z/c), \qquad (73)$$

$$B^{(S)}(\nu, \delta_B) = -\frac{I}{2}r_{ref}r_{sam}\sin 2\theta \cos(4\pi\nu\delta_z/c). \qquad (74)$$
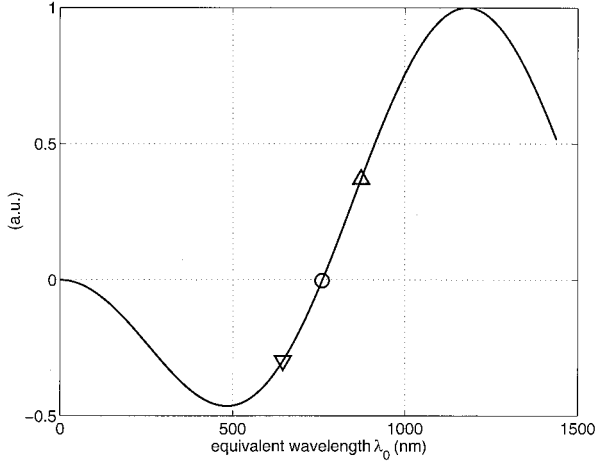
Fig. 4. Value of Eq. (76) as a function of the reference mirror's modulation amplitude: circle, point for calculating Fig. 5(b); triangles, points used in Figs. 5(a) and 5(c).

Equation (72) cannot be made independent of δ_z whatever its value, but we can try to make our notation insensitive to δ_z near a particular value, for example, $\delta_z = 0$. We want to find $\delta_{0\text{opt}}$ that satisfies the equation

$$\frac{d}{d\delta_z}\left[\Sigma_A^{(S)2} + \Sigma_B^{(S)2}\right]\Bigg|_{\delta_z \approx 0} = 0, \tag{75}$$

or, substituting Eqs. (73) and (74) into Eq. (72),

$$\left[\int_0^\infty f(\nu)\Gamma_A(\nu, \delta_{0\text{opt}})\nu d\nu\right]^2$$

$$- \left[\int_0^\infty f(\nu)\Gamma_B(\nu, \delta_{0\text{opt}})d\nu \int_0^\infty f(\nu)\Gamma_B(\nu, \delta_{0\text{opt}})\nu^2 d\nu\right]$$

$$= 0. \tag{76}$$

We can verify that, when $f(\nu)$ is the Dirac distribution $\delta(\nu - \nu_0)$, we end with $\Gamma_A^{(S)} = \Gamma_B^{(S)}$. For an arbitrary spectrum the equation must be solved numerically. The left-hand side of Eq. (76) is plotted in Fig. 4. It was calculated from the flat spectrum from 650 to 950 nm. The first zero of this function gives the value of δ_0, which makes Eq. (72) independent of δ_z near $\delta_z = 0$. One can perform this calculation experimentally as in the monochromatic case by tilting the reference mirror to obtain Fizeau fringes and then finding the value of δ_0 that make the fringes at the center of the interferogram disappear. The width of this region, Δ_z, is nearly equal to the coherence length of the source. Figure 5 shows a calculation of such an interferogram, in which δ_z varies from -2 to $+2$ μm and δ_0 varies from 0.85 to 1.15 times its optimal value. We can clearly see the central fringes disappear as δ_0 reaches its optimal value.
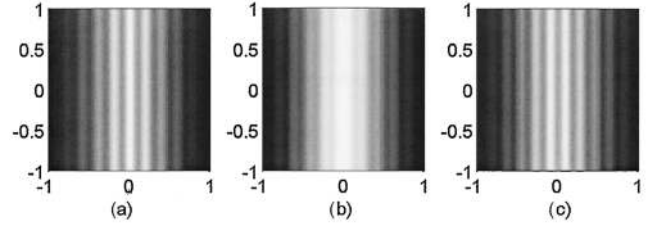

Fig. 5. Simulation of the procedure proposed for fixing the value of δ_0: interferograms with micrometer times micrometer dimensions: (a) $\delta_0 = 0.85 \times \delta_{0\text{opt}}$, (b) $\delta_0 = \delta_{0\text{opt}}$, and (c) $\delta_0 = 1.15 \times \delta_{0\text{opt}}$.

From the value of $\delta_{0\text{opt}}$ we can calculate an equivalent wavelength λ_0, defined by

$$\Gamma_A\left(4\pi \frac{\delta_{0\text{opt}}}{\lambda_0}, \frac{\pi}{4}\right) = \Gamma_B\left(4\pi \frac{\delta_{0\text{opt}}}{\lambda_0}, \frac{\pi}{4}\right). \tag{77}$$

The equivalent wavelength can be thought of as the wavelength that should be used in the monochromatic case with the same modulation amplitude $\delta_{0\text{opt}}$.

Once the values of δ_0 and ψ are fixed we can try to generalize Eq. (54) to encompass a broadband source. We define Θ_A and Θ_B by

$$\Theta_A(\delta_{0\text{opt}}) = \int_0^\infty f(\nu)\Gamma_A\left[\left(\nu, \delta_{0\text{opt}}, \frac{\pi}{4}\right)\right]d\nu,$$

$$\Theta_B(\delta_{0\text{opt}}) = \int_0^\infty f(\nu)\Gamma_B\left[\left(\nu, \delta_{0\text{opt}}, \frac{\pi}{4}\right)\right]d\nu \tag{78}$$

and estimate birefringence δ_B by using

$$\tan^2\left(\pi \frac{\delta_B}{\lambda_0}\right) = \tan^{-2}(2\theta)$$

$$\times \frac{[\Theta_B(\delta_{0\text{opt}})\Sigma_A^{(P)}]^2 + [\Theta_A(\delta_{0\text{opt}})\Sigma_B^{(P)}]^2}{[\Theta_B(\delta_{0\text{opt}})\Sigma_A^{(S)}]^2 + [\Theta_A(\delta_{0\text{opt}})\Sigma_B^{(S)}]^2}, \tag{79}$$

topography δ_z with

$$\tan\left(2\pi \frac{\delta_z}{\lambda_0}\right) = \frac{\Theta_B(\delta_{0\text{opt}})\Sigma_A^{(S)}}{\Theta_A(\delta_{0\text{opt}})\Sigma_B^{(S)}}, \tag{80}$$

and the birefringence direction as

$$\tan(2\beta) = \frac{\Theta_A(\delta_{0\text{opt}})\Theta_B(\delta_{0\text{opt}})[\Sigma_A^{(S)}\Sigma_B^{(P)} - \Sigma_A^{(P)}\Sigma_B^{(S)}]}{\Theta_A^2(\delta_{0\text{opt}})\Sigma_B^{(S)}\Sigma_B^{(P)} + \Theta_B^2(\delta_{0\text{opt}})\Sigma_A^{(S)}\Sigma_A^{(P)}}. \tag{81}$$

For a monochromatic source, only the measurement of the direction of birefringence axes β was affected by the topography. For the broadband source, neither β nor δ_B can be made rigorously independent of δ_z. Figure 6 shows the calculated value of the topography plotted relative to the true topography. Figure 7 shows the minimum and maximum values of the estimated birefringence as functions of the true birefringence for two values of the birefringence direction, as δ_z varies from $\delta_z = 0$ to $\delta_z = 0.75 \times \lambda_0$.
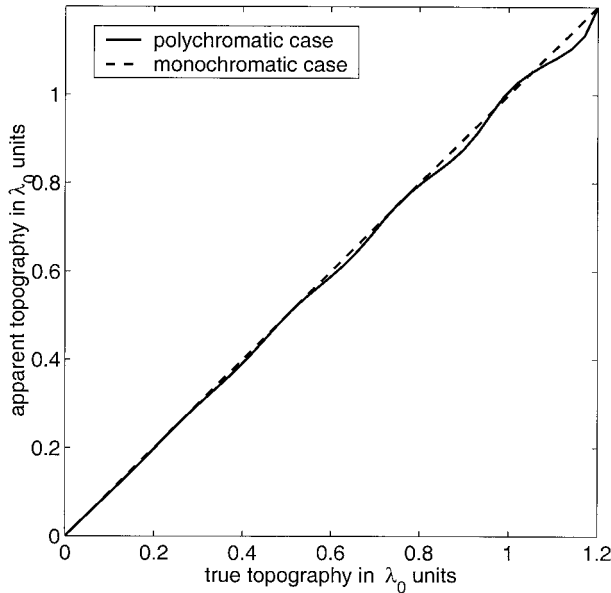
Fig. 6. Estimated versus true topography δ_z for a source spectrum that is flat from 650 to 950 nm.

The estimation error depends on the value of δ_z. For values of $\delta_z > \Delta_z/2$, Eqs. (79)–(81) cannot be used. This simply means that, outside the coherence length of the source, the measurement cannot be made, which is a standard limitation of phase detection methods.[25] A way to overcome this limitation is first to perform a test on the interferometer envelope[26] to discriminate between points at which the evaluation birefringence can or cannot give accurate results. One could of course use efficient combinations of more than four images[27,28] to obtain a precise measurement of the coherence envelope, but this test should not be used directly to measure topography, as it would give poor results. Let function Ω be defined by

$$\Omega(\delta_B, \beta, \delta_z) = \Sigma_A^{(S)2} + \Sigma_A^{(P)2} + \Sigma_B^{(S)2} + \Sigma_B^{(P)2}. \quad (82)$$

Figure 8 is a plot of the maximum and minimum values of Ω as functions of δ_z when φ_B takes the
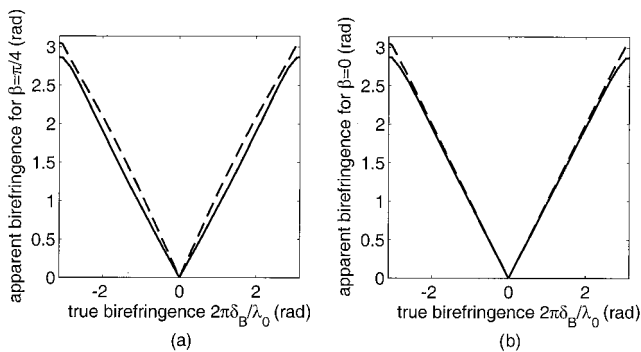

Fig. 7. Magnitudes of estimated versus true birefringence δ_B for various values of topography δ_z ranging from 0 (dashed curves) to $0.75 \times \lambda_0$ (solid curves) for the flat source spectrum: (a) $\beta = \pi/4$, (b) $\beta = 0$.
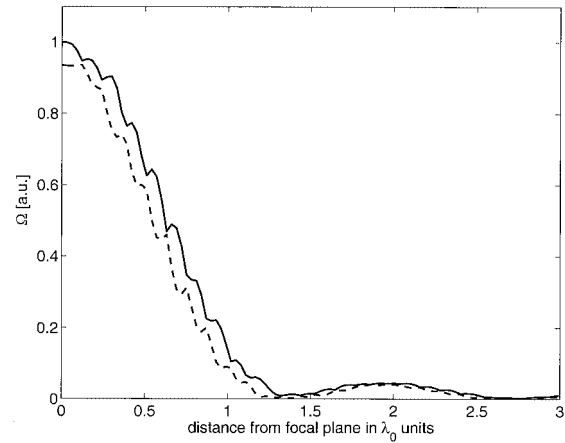

Fig. 8. Values of Ω as a function of δ_z expressed in units of λ_0 for $\varphi_B = 0$ (solid curve) and $\varphi_B = \pi$ (dashed curve).

values 0 and π rad. We see that Ω is only slightly dependent on the birefringence. Ω can thus be used as an estimate of the coherence envelope. By calculating the value of this function at each point on the image field we roughly estimate the topography, independently of the birefringence. In practice, for recording full-field images, one fixes the sample upon an axial translation stage that permits step-by-step movement with step size d_z smaller than the FWHM of Ω. For a given position of the sample, the birefringence is evaluated only inside the region where the rough topography has a value smaller than $d_z/2$. This condition determines the threshold level that is used with the function Ω.

4. Discussion

We have presented a method for combining phase-sensitive OCT and thermal-light OCT to obtain polarization-sensitive tomographic images. We have shown that, within determined limits, birefringence or dichroism and a tomographic phase can be measured nearly independently of each other. A combination of coherence envelope detection and tomographic phase measurement permits discrimination between points where the evaluation of birefringence is strongly dependent on topography and points where simple formulas can be used to obtain accurate results. We have presented formulas that explicitly include the spectrum of the light source and allow us to evaluate birefringence by use of a thermal-light polarization-sensitive optical coherence tomography instrument. Micrometer axial resolution is then possible with such a white-light source. These formulas [Eqs. (79)–(81)] are simple combinations of eight images; they hide the experimental difficulties introduced by the use of imperfectly achromatic components and by the need to combine two different arrangements of polarizing elements. The polarization scheme used rejects light whose polarization state has not been modified by the sample. This property, combined with micrometer resolution, makes this instrument a valuable tool for

the study of small-scale birefringent defects inside optical components, in particular, inside optical multilayer coatings. Although our primary motivation for developing this measurement method was to use it for the study of optical components, biological applications could of course also benefit from it.

References

1. J. M. Mackowski, L. Pinard, L. Dognin, P. Ganau, B. Lagrange, C. Michel, and M. Morgue, "Different approaches to improve the wavefront of low-loss mirrors used in the VIRGO gravitational wave antenna," Appl. Surf. Sci. **151,** 86–90 (1999).
2. J.-Y. Vinet, V. Brisson, S. Braccini, I. Ferrante, L. Pinard, F. Bondu, and E. Tourni, "Scattered light noise in gravitational wave interferometric detectors: a statistical approach," Phys. Rev. D **56,** 6085–6095 (1997).
3. L. Vabre, V. Loriette, A. Dubois, J. Moreau, and A. C. Boccara, "Imagery of local defects in multilayer components by short coherence length interferometry," Opt. Lett. **27,** 1899–1901 (2002).
4. J. F. de Boer, T. E. Milner, M. J. C. van Gemert, and J. S. Nelson, "Two-dimensional birefringence imaging in biological tissue by polarization-sensitive optical coherence tomography," Opt. Lett. **22,** 934–936 (1997).
5. J. F. de Boer, S. M. Srinivas, A. Malekafzali, Z. Chen, and J. S. Nelson, "Imaging thermally damaged tissue by polarization sensitive optical coherence tomography," Opt. Express **3,** 212–218 (1998), http://www.opticsexpress.org.
6. M. J. Everett, K. Schoenenberger, B. W. Colston, Jr., and L. B. Da Silva, "Birefringence characterization of biological tissue by use of optical coherence tomography," Opt. Lett. **23,** 228–230 (1998).
7. K. Schoenenberger, B. W. Colston, Jr., D. J. Maitland, L. B. Da Silva, and M. J. Everett, "Mapping of birefringence and thermal damage in tissue by use of polarization-sensitive optical coherence tomography," Appl. Opt. **37,** 6026–6036 (1998).
8. J. F. de Boer, T. E. Milnerand, and J. S. Nelson, "Determination of the depth-resolved Stokes parameters of light backscattered from turbid media by use of polarization-sensitive optical coherence tomography," Opt. Lett. **24,** 300–302 (1999).
9. G. Yao and L. V. Wang, "Two-dimensional depth-resolved Mueller matrix characterization of biological tissue by optical coherence tomography," Opt. Lett. **24,** 537–539 (1999).
10. C. E. Saxer, J. F. de Boer, B. H. Park, Y. Zhao, Z. Chen, and J. S. Nelson, "High-speed fiber-based polarization-sensitive optical coherence tomography of *in vivo* human skin," Opt. Lett. **25,** 1355–1357 (2000).
11. C. K. Hitzenberger, E. Götzinger, M. Sticker, M. Pircher, and A. F. Fercher, "Measurement and imaging of birefringence and optic axis orientation by phase resolved polarization sensitive optical coherence tomography," Opt. Express **9,** 780–790 (2001), http://www.opticsexpress.org.
12. J. E. Roth, J. A. Kozak, S. Yazdanfar, A. M. Rollins, and J. A. Izatt, "Simplified method for polarization-sensitive optical coherence tomography," Opt. Lett. **26,** 1069–1071 (2001).
13. W. Drexler, U. Morgner, F. X. Kärtner, C. Pitris, S. A. Boppart, X. D. Li, E. P. Ippen, and J. G. Fujimoto, "*In vivo* ultrahigh-resolution optical coherence tomography," Opt. Lett. **24,** 1221–1223 (1999).
14. A. M. Kowalevicz, T. Ko, I. Hartl, J. G. Fujimoto, M. Pollnau, and R. P. Salathé, "Ultrahigh resolution optical coherence tomography using a superluminescent light source," Opt. Express **10,** 349–353 (2002), http://www.opticsexpress.org.
15. L. Vabre, A. Dubois, and A. C. Boccara, "Thermal-light full-field optical coherence tomography," Opt. Lett. **27,** 530–532 (2002).
16. P. de Groot and L. Deck, "Surface profiling by analysis of white-light interferograms in the spatial frequency domain," J. Mod. Opt. **42,** 389–401 (1995).
17. E. Beaurepaire, A. C. Boccara, M. Lebec, L. Blanchot, and H. Saint-Jalmes, "Full-field optical coherence microscopy," Opt. Lett. **23,** 244–246 (1998).
18. A. Dubois, L. Vabre, A.-C. Boccara, and E. Beaurepaire, "High-resolution full-field optical coherence tomography with a Linnick microscope," Appl. Opt. **41,** 805–812 (2002).
19. A. Dubois, L. Vabre, and A. C. Boccara, "Sinusoidally phase-modulated interference microscope for high-speed high-resolution topographic imagery," Opt. Lett. **26,** 1873–1875 (2001).
20. A. Dubois, "Phase-map measurements by interferometry with sinusoidal phase modulation and four integrating buckets," J. Opt. Soc. Am. A **18,** 1972–1979 (2001).
21. L. Vabre, A. Dubois, M. C. Potier, J. L. Stehlé, and A. C. Boccara, "DNA microarray inspection by interference microscopy," Rev. Sci. Instrum. **72,** 2834–2836 (2001).
22. A. Dubois, J. Selb, L. Vabre, and A.-C. Boccara, "Phase measurements with wide-aperture interferometers," Appl. Opt. **39,** 2326–2331 (2000).
23. E. Collett, *Polarized Light: Fundamental and Applications*, Vol. 36 of Optical Engineering Series (Marcel Dekker, New York, 1993).
24. J. F. Mosiño, A. Starodumov, O. Barbosa-García, and V. N. Filippov, "Propagation of partially polarized light in dichroic and birefringent media," J. Opt. B **3,** 159–165 (2001).
25. P. Hariharan and M. Roy, "White-light phase stepping interferometry: measurement of the fractional interference order," J. Mod. Opt. **42,** 2357–2360 (1995).
26. A. Harasaki, J. Schmit, and J. C. Wyant, "Improved vertical-scanning interferometry," Appl. Opt. **39,** 2107–2115 (2000).
27. K. G. Larkin, "Efficient nonlinear algorithm for envelope detection in white light interferometry," J. Opt. Soc. Am. A **13,** 832–843 (1996).
28. P. Sandoz, "An algorithm for profilometry by white-light phase-shifting interferometry," J. Mod. Opt. **43,** 1545–1554 (1996).